

# Influence of a superficial layer in the quantitative spectroscopic study of strongly scattering media

Maria Angela Franceschini, Sergio Fantini, L. Adelina Paunescu, John S. Maier, and Enrico Gratton

We have experimentally investigated the meaning of the effective optical absorption [ $\mu_a^{(\text{eff})}$ ] and the reduced scattering [ $\mu_s'^{(\text{eff})}$ ] coefficients measured on the surfaces of two-layered turbid media, using the diffusion equation for homogeneous, semi-infinite media. We performed frequency-domain spectroscopy in a reflectance geometry, using source-detector distances in the range 1.5–4.5 cm. We measured 100 samples, each made of one layer (thickness in the range 0.08–1.6 cm) on top of one semi-infinite block. The optical properties of the samples were similar to those of soft tissues in the near infrared. We found that the measured effective optical coefficients are representative of the underlying block if the superficial layer is less than ~0.4 cm thick, whereas they are representative of the superficial layer if it is more than ~1.3 cm thick. © 1998 Optical Society of America

OCIS codes: 170.5280, 170.6510, 170.7050, 300.0300, 300.6340.

## 1. Introduction

Near-infrared (700–900 nm) spectroscopy is a noninvasive technique by which one can investigate biological tissues to depths of several centimeters.<sup>1,2</sup> For instance, the human breast can be transilluminated through a thickness of approximately 4–8 cm.<sup>3–5</sup> In reflection geometry, i.e., with the light source and the optical detector on the same side of the tissue, skeletal muscles<sup>6–8</sup> and the human brain<sup>9,10</sup> can be probed to a depth of ~2 cm. The introduction of a physical model (diffusion theory) to describe light propagation in tissues<sup>11</sup> has led to quantitative tissue spectroscopy, which opened new possibilities in the field of optical diagnostics. For instance, recent achievements include the quantitative assessment of hemoglobin concentration and saturation in tissue, in conjunction with the absolute measurement of the tissue's reduced scattering coefficient  $\mu_s'$ .<sup>12–14</sup> This parameter can be influenced by changes in several physiological conditions, including blood glucose concentration.<sup>15–17</sup> The physical model used to de-

scribe the diffuse reflectance in tissues is usually the diffusion equation for homogeneous, semi-infinite media. Because biological tissues are not spatially homogeneous, this model may not be adequate. In particular, tissue inhomogeneities become important when they occur on a spatial scale greater than or of the order of the distance over which the photon direction is randomized. This distance, which is given by  $1/\mu_s'$ , is ~0.1 cm in most tissues. Superficial tissue layers such as the skin, the subcutaneous fat layer, and the skull constitute optical inhomogeneities that have typical thicknesses of the order of several millimeters. Given that the presence of these superficial layers cannot be avoided in noninvasive applications, it is relevant to study their influence on quantitative tissue spectroscopy.

The diffuse reflectance in two-layered, strongly scattering media was obtained by computer simulations of a lattice random walk for two layers that have the same lattice spacing (i.e., the same scattering probability) but different absorption probabilities.<sup>18</sup> An analytical approximation of the reflected intensity was derived in the special case of an upper layer that is more absorbing than the lower layer.<sup>19</sup> Diffusion theory can be employed to describe light propagation in multilayered turbid media. This approach involves a system of diffusion equations (one for each layer) and the appropriate boundary conditions for the photon fluence rate and for the normal component of the photon flux at the interface between adjacent layers.<sup>20,21</sup> The diffusion-theory approach, in con-

---

The authors are with the Laboratory for Fluorescence Dynamics, Department of Physics, University of Illinois at Urbana—Champaign, 1110 West Green Street, Urbana, Illinois 61801-3080. S. Fantini's e-mail address is fantini@uiuc.edu.

Received 21 April 1998; revised manuscript received 27 July 1998.

0003-6935/98/317447-12\$15.00/0  
© 1998 Optical Society of America

junction with a Fourier-transform method, has led to an expression for the spatially resolved reflectance in two-layered media<sup>22</sup> that has been verified to be in good agreement with Monte Carlo simulations in the time and frequency domains and with continuous-wave (cw) experimental data.<sup>23</sup> Diffusion theory and Monte Carlo simulations were employed to investigate the influence of a layered tissue structure on the determination of the optical properties from steady-state and time-resolved diffuse reflectometry.<sup>24</sup> Hielscher *et al.* conducted an experimental study of two-layered phantoms in the time domain.<sup>25</sup> This study showed that the tail of the photon time-of-flight distribution measured at a source–detector separation greater than 1 cm is weakly affected by the presence of a superficial layer less than 1 cm thick. As a result, the absorption coefficient ( $\mu_a$ ) of the underlying medium can be accurately determined in the time domain, even in the presence of the superficial layer. Homma *et al.* applied cw spectroscopy to muscles *in vivo* to investigate the influence of the subcutaneous adipose tissue layer on the optical penetration depth.<sup>8</sup> Near-infrared light was found to penetrate to a depth at least equal to half of the source–detector separation, even in the presence of an adipose tissue layer as much as 1.0 cm thick.

Here we experimentally investigate the effect of a superficial layer on quantitative optical measurements conducted in reflection geometry. Our approach is not based on computer simulations or on a generalization of diffusion theory to treat the layered inhomogeneity of the sample. By contrast, we use the diffusion equation for semi-infinite, homogeneous media to obtain the effective optical coefficients [ $\mu_a^{(\text{eff})}$  and  $\mu_s'^{(\text{eff})}$ ] of the two-layered media. In our experimental study we seek to answer the question: What is the meaning of these effective optical coefficients, i.e., how are they related to the optical properties of the superficial layer and the underlying medium? The answer to this question should depend on the measurement protocol that we use to obtain  $\mu_a^{(\text{eff})}$  and  $\mu_s'^{(\text{eff})}$ , so we have considered both multidistance and single-distance measurement protocols. The rationale for our approach is as follows: The geometrical distribution of the tissue's optical properties is extremely irregular, is not well known, and varies from subject to subject. Consequently, any assumption about a regular tissue geometry (for instance, a two-layered structure, with the top layer having a constant thickness) would be somewhat arbitrary and should not be expected to be realistic. Furthermore, the diffusion-theory approach requires that the sample size be much larger than the photon's mean free path. This condition may not be satisfied if thin layers ( $\sim 0.1$  cm thick) are considered. Finally, to use diffusion theory to obtain the optical properties of both layers one needs to measure the spatially resolved reflectance over a wide range of source–detector distances, an objective that may not be practical to achieve. Therefore we decided to investigate the conditions under which different measurement protocols based on the equations for semi-

infinite, uniform media are affected by a specific perturbation to the spatial homogeneity or to the semi-infinite geometry. Following this approach, we recently investigated the effect of curved boundaries on quantitative tissue spectroscopy.<sup>26</sup> Here we study how a superficial layer of thickness ranging from 0.08 to 1.6 cm affects the effective optical properties obtained from optical data collected at source–detector separations in the range 1.5–4.5 cm.

## 2. Experimental Methods

### A. Samples

The strongly scattering samples were made of gelatin (Grayslake Gelatin Company, Grayslake, Ill.), to which we added various amounts of titanium dioxide (TiO<sub>2</sub>) particles (Liquitex, Binney & Smith, Inc., Easton, Pa.) and black India ink (black India 4415, Eberhard Faber, Inc., Lewisburg, Tenn.). By selecting the amount of TiO<sub>2</sub> particles and black India ink, we were able to produce samples that had different values of the reduced scattering coefficient ( $\mu_s'$ ) and the absorption coefficient ( $\mu_a$ ). We prepared five batches of gelatin, which we labeled 1–5, each having a different pair of absorption and reduced scattering coefficients. From each of these five batches we cast one block with a size of approximately 20 cm (L)  $\times$  10 cm (W)  $\times$  5 cm (D) and four layers with a thickness in the range 0.08–1.6 cm (and approximately the same length and width as the rectangular blocks). From now on, we identify the rectangular blocks simply as blocks, and the layers, which in the measurements were placed on top of the blocks, simply as layers. The optical properties of the blocks [ $\mu_a^{(B)}$ ,  $\mu_s'^{(B)}$ ] at 750 nm were measured with a frequency-domain spectrometer (see Subsections 2.B and 4.A), and they are shown in Fig. 1. In Fig. 1 the numbers in parentheses represent the measurement error in the last digit of the corresponding parameter and give an indication of the accuracy in the optical coefficients. The optical properties of the layers [ $\mu_a^{(L)}$ ,  $\mu_s'^{(L)}$ ] are the same as the optical properties of the corresponding blocks because they are made from the same gelatin batch. Figure 1 also gives the depths of all the blocks and the thicknesses of all the layers. The uncertainty in the layer thicknesses, which includes both the measurement error and the nonuniformity of the layer thickness, is  $\sim 10\%$ .

In our measurements we placed the optical probe containing the source fibers and the detector fibers on the upper sides of the blocks (or of a layer–block combination), as described in Subsection 2.B. Therefore we worked in a diffuse-reflectance geometry. In these conditions the average photon-visit depth  $\langle z \rangle$ , at a source–detector separation  $r$ , can be estimated from the empirical relationship

$$\langle z \rangle = \frac{1}{2} \left[ \frac{r}{(3\mu_a\mu_s')^{1/2}} \right]^{1/2} \quad (1)$$

derived by Patterson *et al.*<sup>27</sup> In our measurements the maximum value of  $\langle z \rangle$ , which corresponds to our

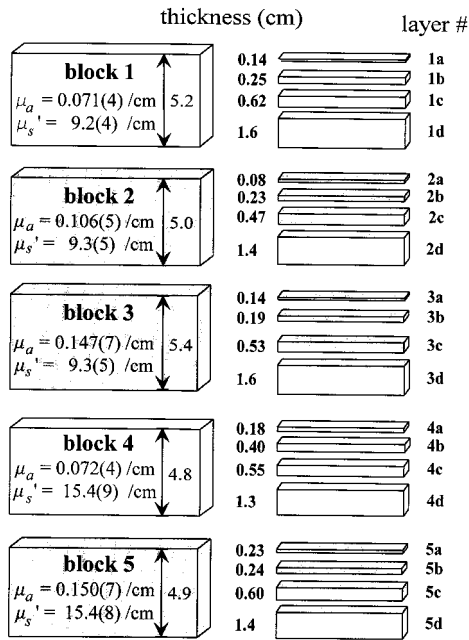


Fig. 1. Effectively semi-infinite blocks and layers employed in our experimental study. The blocks and the layers are composed of five batches of gelatin (labeled 1–5), each having a different amount of  $\text{TiO}_2$  particles and black India ink. The optical properties of each batch at 750 nm are indicated inside the blocks. The numbers in parentheses give the error in the last digit of the corresponding parameter. The thickness of each block and layer is also shown. We carried out measurements on all the 100 combinations of one layer on top of one block.

largest  $r$  (4.5 cm), the smallest  $\mu_a$  ( $0.07 \text{ cm}^{-1}$ ), and the smallest  $\mu_s'$  ( $9.2 \text{ cm}^{-1}$ ), is  $\sim 0.9 \text{ cm}$ . As the depth of the blocks exceeds this value by many diffusion lengths (the diffusion length is the decay length of the photon density in the blocks, and it is approximately

0.4–0.7 cm in our samples), we can consider the blocks to be effectively semi-infinite media.

We carried out a study of two-layered media by considering all possible combinations (100) of one layer on top of one block. Because the blocks and the layers are all made from the same material, there is no refractive-index mismatch at the interface between the block and the layer. It is helpful to divide the large number of layer–block combinations into four categories, according to the relative values of the optical coefficients of the layer and the block:

- (1) Same  $\mu_a$ , same  $\mu_s'$ :  $\mu_a^{(L)} = \mu_a^{(B)}$  and  $\mu_s'^{(L)} = \mu_s'^{(B)}$ ,
- (2) Same  $\mu_a$ , different  $\mu_s'$ :  $\mu_a^{(L)} = \mu_a^{(B)}$  and  $\mu_s'^{(L)} \neq \mu_s'^{(B)}$ ,
- (3) Different  $\mu_a$ , same  $\mu_s'$ :  $\mu_a^{(L)} \neq \mu_a^{(B)}$  and  $\mu_s'^{(L)} = \mu_s'^{(B)}$ ,
- (4) Different  $\mu_a$ , different  $\mu_s'$ :  $\mu_a^{(L)} \neq \mu_a^{(B)}$  and  $\mu_s'^{(L)} \neq \mu_s'^{(B)}$ .

### B. Frequency-Domain Spectrometer

The data were acquired with a frequency-domain spectrometer designed for applications in tissue oximetry (ISS, Inc., Champaign, Ill., Model 96208), whose light sources are modulated at a frequency of 110 MHz (Ref. 28); Fig. 2. The quantities measured by this instrument are the average value (dc), the amplitude (ac), and the phase ( $\Phi$ ) of the detected 110-MHz intensity wave. This instrument is equipped with two independent channels (channel a and channel b) that provide dual parallel acquisition. Each channel consists of eight laser diodes, four emitting at 750 nm and four at 840 nm, which are electronically multiplexed at a rate of 50 Hz, so only one of them is on (for 20 ms) at a time. Each laser diode is coupled to an optical fiber (source fiber) that has a core diam-

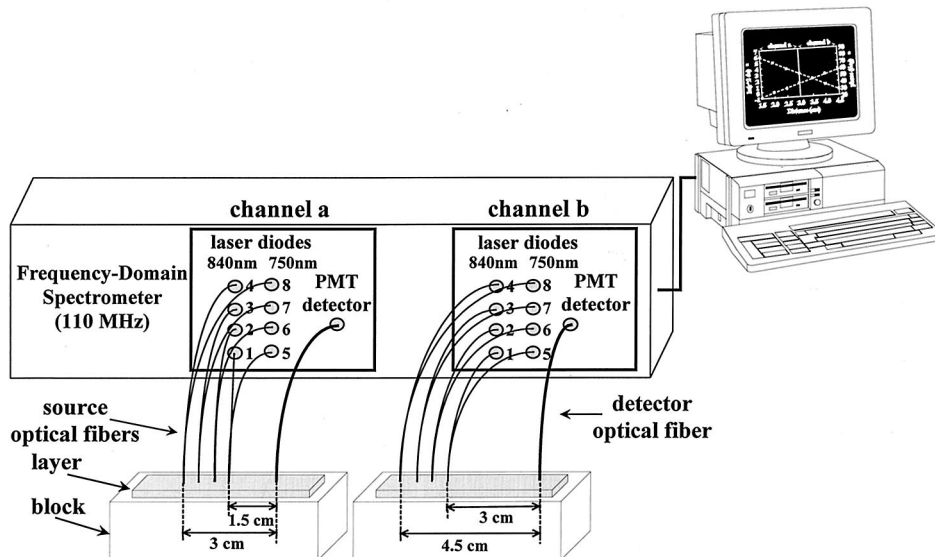


Fig. 2. Experimental arrangement. The frequency-domain data (dc, ac, and phase) were measured on top of the layer–block combination over the range of distances 1.5–3.0 cm (channel a) and 3.0–4.5 cm (channel b). PMT's, photomultiplier tubes; 110 MHz is the modulation frequency of the intensity of the light sources.

eter of 600  $\mu\text{m}$ . An optical fiber bundle 3 mm in diameter (detector fiber) is used to collect the optical signal and to send it to a photomultiplier tube detector (one per channel). The source fibers and the detector fiber are arranged in a planar measuring probe in such a way that the instrument can acquire data on the surface of the sample at four different source-detector separations ( $r$ ). The only difference between channels a and b is that channel a acquired data at  $r$  ranging from 1.5 to 3.0 cm, whereas channel b acquired data in the range 3.0–4.5 cm (see Fig. 2). To account for the different emission properties of the eight light sources (per channel), this instrument requires a preliminary measurement on a calibration pad [size, 14 cm (L)  $\times$  8 cm (W)  $\times$  4 cm (D)] with known optical properties<sup>12</sup> [ $\mu_a = 0.11$  (0.18)  $\text{cm}^{-1}$ ,  $\mu_s' = 6.5$  (5.6)  $\text{cm}^{-1}$  at 750 (840) nm]. Figure 2 is a schematic diagram of the experimental arrangement.

The acquisition time, i.e., the measurement time to get the frequency-domain data (dc, ac, and phase) at the four detector separations and at both wavelengths, was set to 2.56 s. The resultant standard deviation errors in dc, ac, and phase were approximately 0.5%, 0.5%, and 0.1°, respectively. In all the measurements the dc voltage at the photomultiplier tube, which determines its gain, was never changed. It was  $\sim 550$  V for channel a and  $\sim 850$  V for channel b. By keeping the PMT gain fixed we could compare the intensity and phase data collected on different samples. By repeatedly repositioning the optical probe on the calibration pad during the course of the measurement session we verified the stable emission properties (dc, ac, and phase) of the laser diodes and the good reproducibility of the probe-sample optical contact. We found overall reproducibilities in dc, ac, and phase to within 5%, 5%, and 0.5°, respectively, during the duration of the experiment. The information content of the data at the two wavelengths (750 and 840 nm) turned out to be similar, so we show only our results at 750 nm.

### 3. Main Features of the Diffuse Reflectance in Two-Layered Media

Figure 3 illustrates the  $r$  dependence of the diffuse reflectance in five cases: three two-layered media (one superficial layer on top of one block) with different thicknesses of the superficial layer (thin lines) and two semi-infinite, homogeneous media that have the optical properties of either the layer or the block (thick lines). This figure was generated from the solution provided by diffusion theory for two-layered media.<sup>23</sup> The  $y$  axis of Fig. 3 represents  $\ln(r^2 \text{dc})$ , which, to a first approximation, gives a straight line versus  $r$  in homogeneous semi-infinite media. (More rigorously, the straight line is given by a function  $f$ , which is introduced in Subsection 4.A.) Multidistance methods rely on the slope of this line to derive the optical coefficients (which should be called effective optical coefficients in the case of inhomogeneous media). Single-distance methods use the absolute value of the reflectance measured at one particular

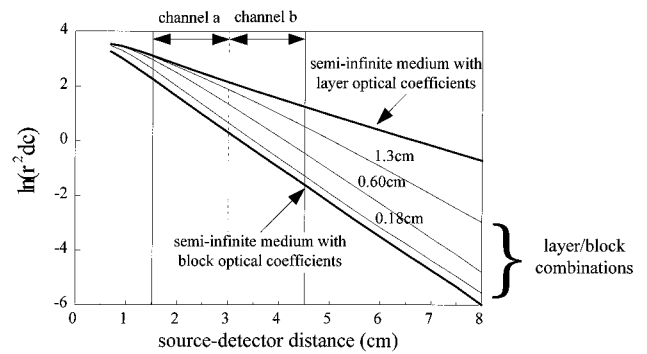


Fig. 3. Dependence of  $\ln(r^2 \text{dc})$  on source-detector distance for five different media. Thick lines, semi-infinite, homogeneous media that have either the layer optical coefficients [upper curve,  $\mu_a^{(L)} = 0.017 \text{ cm}^{-1}$ ,  $\mu_s'^{(L)} = 5.4 \text{ cm}^{-1}$ ] or the block optical coefficients [lower curve,  $\mu_a^{(B)} = 0.070 \text{ cm}^{-1}$ ,  $\mu_s'^{(B)} = 7.3 \text{ cm}^{-1}$ ]. Thin lines, three layer-block configurations that differ in layer thickness. The layer thickness is indicated next to each line. The media considered in this figure are less attenuating than those employed in our experimental study. The lines in this figure were calculated from the solution of diffusion theory for two-layered media reported by Kienle *et al.*<sup>23</sup>

source-detector separation to obtain the (effective) optical coefficients.

There are several features illustrated by Fig. 3:

(1) In the presence of a superficial layer, increasing  $r$  causes a gradual change in the slope of  $\ln(r^2 \text{dc})$ , from the slope that corresponds to the layer coefficients to the slope that corresponds to the block coefficients. This fact indicates that the multidistance method performed at short (large) distances will recover the layer's (block's) optical properties.

(2) In the ranges of distances considered in our measurements (1.5–3.0 cm for channel a and 3.0–4.5 cm for channel b), the curvature of function  $\ln(r^2 \text{dc})$  is small. Therefore it is meaningful to obtain the effective optical coefficients with the multidistance method based on the slope of  $\ln(r^2 \text{dc})$  (or, more rigorously, on function  $f$  of Subsection 4.A).

(3) Even a relatively thin superficial layer, 0.18 cm thick, causes a significant change in the absolute reflectance at any given value of  $r$ , so the effective optical coefficients measured with single-distance methods will not, in general, accurately reproduce the block's optical coefficients.

(4) In principle, one can use the rigorous solution of diffusion theory for two-layered media to measure the thickness of the layer and the optical properties of both the layer and the block. However, doing this will require measurement of the diffuse reflectance over a range of distances where  $\ln(r^2 \text{dc})$  shows significant curvature. Figure 3 shows that such a range of distances is greater than that employed by us in either channel a or channel b and may not be practical in biomedical applications *in vivo* (because of the effect of other kinds of inhomogeneity and because of dynamic-range and signal-to-noise ratio considerations).

#### 4. Data Analysis

##### A. Frequency-Domain Multidistance Method (Absolute Measurement)

To derive the effective absorption  $[\mu_a^{(\text{eff})}]$  and the reduced scattering  $[\mu_s'^{(\text{eff})}]$  coefficients from the dc and the phase data acquired at multiple source–detector distances  $r$ , we used a previously described method based on the diffusion-equation solution for homogeneous, semi-infinite media.<sup>29</sup> This method is based on measurement of the slopes of the straight lines given by the two functions  $f[r, \text{dc}, \mu_a^{(\text{eff})}, \mu_s'^{(\text{eff})}]$  and  $h[r, \Phi, \mu_a^{(\text{eff})}, \mu_s'^{(\text{eff})}]$  as a function of  $r$ :

$$f[r, \text{dc}, \mu_a^{(\text{eff})}, \mu_s'^{(\text{eff})}] = rS_{\text{dc}}[\mu_a^{(\text{eff})}, \mu_s'^{(\text{eff})}] + K_{\text{dc}}, \quad (2)$$

$$h[r, \Phi, \mu_a^{(\text{eff})}, \mu_s'^{(\text{eff})}] = rS_{\Phi}[\mu_a^{(\text{eff})}, \mu_s'^{(\text{eff})}] + K_{\Phi}, \quad (3)$$

where  $S_{\text{dc}}$  and  $S_{\Phi}$  represent the slopes and  $K_{\text{dc}}$  and  $K_{\Phi}$  are the intercepts that contain the unknown source terms  $\text{dc}_0$  and  $\Phi_0$ . The analytical forms of the functions  $f$  and  $h$  are given in Ref. 29. The choice of dc and phase data, as opposed to ac and phase data, is suggested by a higher signal-to-noise ratio, as discussed in Ref. 30. The effective optical coefficients are determined by the slopes  $S_{\text{dc}}$  and  $S_{\Phi}$  from the following equations:

$$\mu_a^{(\text{eff})} = -\frac{\omega}{2\nu} \frac{S_{\text{dc}}}{S_{\Phi}} \left( \frac{S_{\Phi}^2}{S_{\text{dc}}^2} + 1 \right)^{-1/2}, \quad (4)$$

$$\mu_s'^{(\text{eff})} = \frac{S_{\text{dc}}^2}{3\mu_a^{(\text{eff})}} - \mu_a^{(\text{eff})}, \quad (5)$$

where  $\omega$  is the angular modulation frequency and  $\nu$  is the speed of light in the sample. We solve the difficulty introduced by the dependence of  $f$  and  $h$  on the unknown optical coefficients  $\mu_a^{(\text{eff})}$  and  $\mu_s'^{(\text{eff})}$  by employing an iterative procedure that assigns arbitrary starting values to  $\mu_a^{(\text{eff})}$  and  $\mu_s'^{(\text{eff})}$  and refines their values at each step. This iterative procedure converges [i.e., the  $i$ th iteration produces values of  $\mu_a^{(\text{eff})}$  and  $\mu_s'^{(\text{eff})}$  that differ from those at the  $(i - 1)$ st iteration by less than one tenth of the experimental error] after a few, typically fewer than five, iterations. We have verified that the dc intensity and phase data, in the range of distances considered by us (1.5–4.5 cm), give rise to approximately straight lines for the functions  $f$  and  $h$  versus  $r$ , even in the presence of the superficial layer. This result, which is shown in Fig. 4, allows us to use the frequency-domain multidistance method to obtain the effective optical properties of the layer–block combination. The purpose of this study is to enable us to understand how the effective optical properties recovered with the semi-infinite model are related to the optical properties of the block and of the superficial layer.

##### B. Frequency-Domain Precalibrated Method (Relative Measurements)

The frequency-domain precalibrated method can measure the effective optical coefficients from dc and phase data acquired at a single source–detector sep-

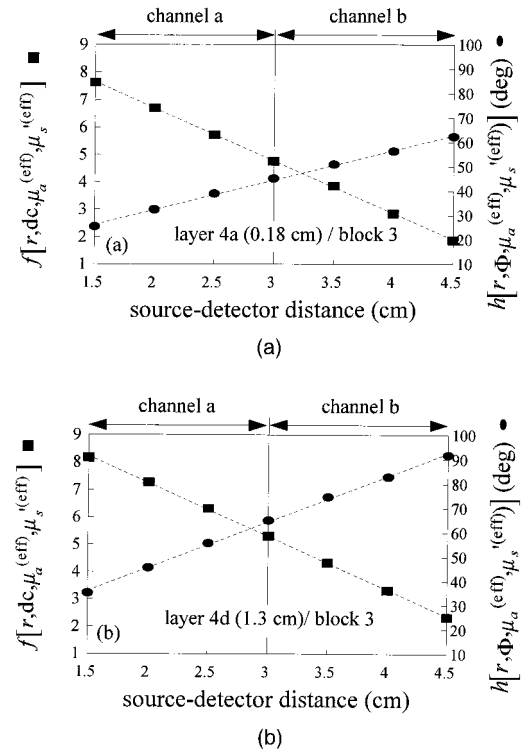


Fig. 4. Squares and circles, the values of the functions  $f[r, \text{dc}, \mu_a^{(\text{eff})}, \mu_s'^{(\text{eff})}]$  and  $h[r, \Phi, \mu_a^{(\text{eff})}, \mu_s'^{(\text{eff})}]$ , respectively, versus source–detector distance  $r$ . As discussed in the text, the fact that  $f$  and  $h$  are approximately described by straight lines (the dashed lines are the best-fit straight lines through the points) allows us to apply the frequency-domain multidistance method to obtain the effective optical properties  $\mu_a^{(\text{eff})}$  and  $\mu_s'^{(\text{eff})}$ . (a) Layer thickness, 0.18 cm; (b) layer thickness 1.3 cm. (a), (b) Layer optical properties are  $\mu_a^{(L4)} = 0.072 \text{ cm}^{-1}$  and  $\mu_s'^{(L4)} = 15.4 \text{ cm}^{-1}$  and block optical properties are  $\mu_a^{(B3)} = 0.147 \text{ cm}^{-1}$  and  $\mu_s'^{(B3)} = 9.3 \text{ cm}^{-1}$ . The data collected with channel b ( $r$  from 3.0 to 4.5 cm) have been normalized to match the data points acquired at  $r = 3.0$  cm by channels a and b.

aration.<sup>31</sup> The basic idea is to derive  $\mu_a^{(\text{eff})}$  and  $\mu_s'^{(\text{eff})}$  from the ratio (difference) between the dc (phase) measured in a medium with known optical properties (precalibration) and in the sample of interest. Taking the dc ratio and the phase difference causes the unknown source terms  $\text{dc}_0$  and  $\Phi_0$  to cancel, and one ends up with two equations (one for the dc and one for the phase) in two unknowns  $[\mu_a^{(\text{eff})}$  and  $\mu_s'^{(\text{eff})}]$ . In principle, this method should provide quantitative measurements of the effective optical properties. However, the absolute values of  $\mu_a^{(\text{eff})}$  and  $\mu_s'^{(\text{eff})}$  obtained with this method showed a dependence on  $r$  even in measurements on the homogeneous, semi-infinite blocks. This result points out a flaw in the precalibrated method that we have assigned to the inadequacy of the assumption of a point-like photon source located at the tip of the source fiber.<sup>32</sup> Despite this limitation, one can still use this method to measure differences in the values of  $\mu_a^{(\text{eff})}$  and  $\mu_s'^{(\text{eff})}$  obtained in two different samples, provided that the optical properties of the samples are similar. In fact, (1) these differences do not show

any  $r$  dependence in the homogeneous blocks alone (whereas there can be an  $r$  dependence in the presence of a layer because the optical properties of the probed volume change at different values of  $r$ ) and (2) the relative measurements in semi-infinite blocks have an accuracy better than 15% in the range of optical properties considered here. The frequency-domain precalibrated method requires that the measured change in the optical coefficients not be large, that the optical coupling with each sample be the same, and that the emission properties of the source (dc and phase) be constant.

### C. Continuous-Wave Differential Path-Length Factor Method (Relative Measurements)

The cw differential path-length factor (DPF) method, which measures changes in the effective absorption coefficient  $\mu_a^{(\text{eff})}$  from changes in the dc intensity, is described in Ref. 33. It is based on two assumptions:

(1) The absorbance, i.e.,  $\ln(I_0/I)$ , where  $I_0$  is the source intensity and  $I$  is the detected intensity after the light has propagated through the medium, can be written as follows:

$$\ln(I_0/I) = \mu_a(\text{DPF})r + G. \quad (6)$$

Here the DPF is defined as the ratio between the mean photon path length and the source–detector separation  $r$ ;  $G$  is a term that depends on the boundary conditions and on the scattering coefficient of the medium. Note that the DPF depends on the reduced scattering coefficient and on the absorption coefficient of the medium.

(2) The DPF and  $G$  are constant during a measurement. This assumption implies that the scattering should remain constant and that the absorption coefficient (which also affects the DPF) should vary only by a small amount during the measurement.

Under the above assumptions, the difference between  $\mu_a^{(\text{eff})}$  for samples 1 and 2 can be written in terms of the ratio  $I_1/I_2$ :

$$\mu_{a2}^{(\text{eff})} - \mu_{a1}^{(\text{eff})} = \frac{1}{r(\text{DPF})} \ln(I_1/I_2). \quad (7)$$

We obtained the value of the DPF for sample 1 from the experimental slope of the phase  $\Phi_1$  versus  $r(d\Phi_1/dr)$  by using the relationship  $\text{DPF} = (v/\omega)d\Phi_1/dr$ . In addition to assumptions (1) and (2) above, the DPF method requires that the optical coupling with each sample be the same and that the source power be constant.

## 5. Results

### A. Absolute Measurements of $\mu_a^{(\text{eff})}$ and $\mu_s'^{(\text{eff})}$ (Frequency-Domain Multidistance Method)

The results obtained for all the 100 layer–block combinations are shown in Fig. 5. The bars in Fig. 5 show the relative deviations between the effective optical coefficients (measured in the presence of the layer) and the block optical coefficients. If we denote

by  $\mu$  either  $\mu_a$  or  $\mu_s'$ , the relative variations are defined as  $[\mu^{(\text{eff})} - \mu^{(B)}]/\mu^{(B)}$ . The black bars refer to measurements with channel a (source–detector distance ranging from 1.5 to 3.0 cm), whereas the gray bars refer to measurements with channel b (source–detector distance ranging from 3.0 to 4.5 cm). The thick horizontal lines represent the relative deviations between the layer and the block optical coefficients {i.e.,  $[\mu^{(L)} - \mu^{(B)}]/\mu^{(B)}$ }, and the number on top of each bar indicates the layer thickness in centimeters.

#### 1. $\mu_a^{(L)} = \mu_a^{(B)}$ and $\mu_s'^{(L)} = \mu_s'^{(B)}$ (Same $\mu_a$ , Same $\mu_s'$ ) [Fig. 5(a)]

As a first step, we verified whether the layer–block interface introduced any artifact. To this end we measured the effective optical coefficients of all the layer–block pairs for which the layer and the block had the same optical properties. Inasmuch as the layer and the block are made from the same material, there is no refractive-index mismatch at the layer–block interface. As shown in Fig. 5(a), the effective absorption coefficient coincides (within experimental errors of  $\pm 10\%$  indicated by the horizontal dashed lines) with the common absorption value of the block and the layer for all the layer thicknesses. The effective reduced scattering coefficient reproduces the common layer–block value in almost all cases. However, as shown in Fig. 5(a),  $\mu_s'^{(\text{eff})}$  deviates from  $\mu_s'^{(B)}$  by more than the experimental error in the seven cases that correspond to the simultaneous occurrence of the following conditions: blocks 2–5, layer thickness in the range 0.23–0.55 cm, and measurements with channel a. We observe that, in these cases, the average photon-visit depth given by Eq. (1) is the smallest ( $\sim 0.52$  cm at  $r = 2.25$  cm) and is of the order of the layer thickness. The deviations between the effective and the true scattering coefficients are always less than 20%. We can conclude that the interface between the layer and the block does not introduce an appreciable effect in the measurement of  $\mu_a^{(\text{eff})}$ , whereas it affects the measurement of  $\mu_s'^{(\text{eff})}$  to within 20%. Consequently, in Figs. 5(b)–5(d) we consider the experimental errors in  $\mu_a^{(\text{eff})}$  and  $\mu_s'^{(\text{eff})}$  to be  $\pm 10\%$  and  $\pm 20\%$ , respectively. These errors are indicated by the horizontal dashed lines in Figs. 5(b)–5(d).

#### 2. $\mu_a^{(L)} = \mu_a^{(B)}$ and $\mu_s'^{(L)} \neq \mu_s'^{(B)}$ (Same $\mu_a$ , Different $\mu_s'$ ) [Fig. 5(b)]

When the layer and the block have the same absorption coefficient but a different reduced scattering coefficient, the measured effective absorption coefficient coincides with the common value in all cases but two: layer 1c on top of block 4 and layer 3c on top of block 5. These are the two cases for which the layer thickness is of the order of the average penetration depth and the layer is less scattering than the block. The effective reduced scattering coefficient coincides with that of the block in the case of thin layers (thickness less than  $\sim 0.5$  cm), whereas it

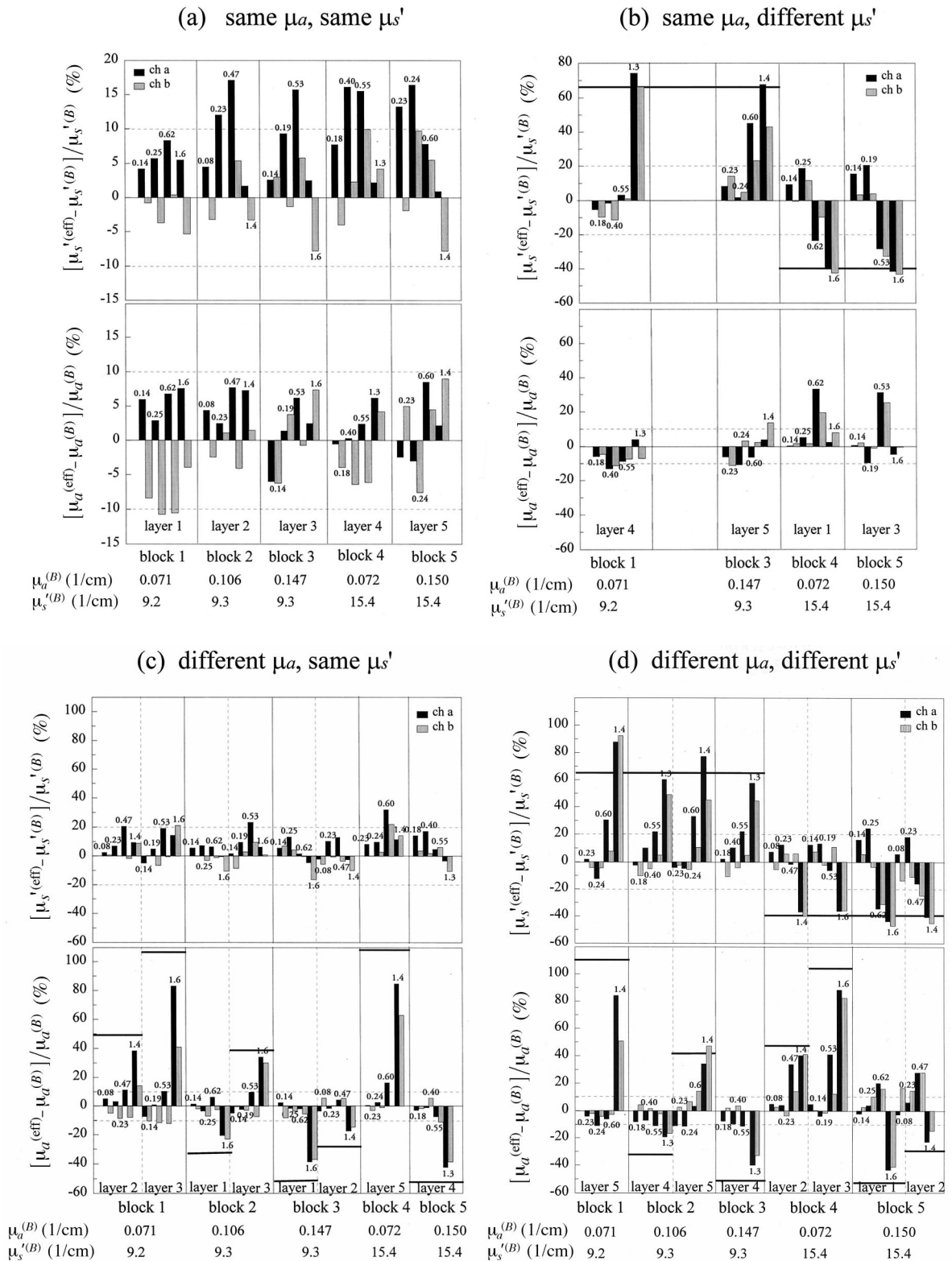


Fig. 5. Summary of our results for all the 100 superficial-layer-underlying-block combinations examined. The black (gray) bars show the percentage deviation between the effective optical properties measured with channel a (channel b) in the presence of one layer, and the corresponding optical properties of the underlying block. The number at the top of each black-gray bar pair indicates the thickness of the layer in centimeters. The horizontal dashed lines indicate the errors. [The instrumental error in the relative deviation is  $\pm 10\%$ . This error is increased to  $\pm 20\%$  for  $\mu_s'$  in (b)–(d) to take into account the effect of the layer-block interface.] The thick horizontal lines indicate the relative deviations (when they are not zero) between the layer and the block optical coefficients. (a) The layer and the block have the same optical coefficients. (b) The layer and the block have the same absorption but different reduced scattering coefficients. (c) The layer and the block have the same reduced scattering but different absorption coefficients. (d) The layer and the block have different absorption and reduced scattering coefficients.

tends to the reduced scattering coefficient of the layer for larger thicknesses. For layers thicker than  $\sim 1.3$  cm,  $\mu_s'^{\text{(eff)}}$  gets close to the reduced scattering coefficient of the layer.

3.  $\mu_a^{(L)} \neq \mu_a^{(B)}$  and  $\mu_s'^{(L)} = \mu_s'^{(B)}$  (Different  $\mu_a$ , Same  $\mu_s'$ ) [Fig. 5(c)]

In the case when the layer and the block have the same reduced scattering coefficient but different absorption coefficients, the measured effective reduced scattering coefficient coincides with the common value in all cases but one: layer 5c on top of block 4. The effective absorption coefficient coincides with that of the block at layer thicknesses of as much as  $\sim 0.6$  cm (the only exception is layer 5c on top of block 4, measured with channel a), whereas it tends to the layer absorption at larger thicknesses. By contrast with the previous case [for which  $\mu_s'^{\text{(eff)}} \approx \mu_s'^{(L)}$  for layer thicknesses greater than 1.3 cm], we observe that, even at a layer thickness of as much as 1.6 cm,  $\mu_a^{(\text{eff})}$  does not reproduce the absorption coefficient of the layer, even though  $\mu_a^{(\text{eff})}$  tends to the layer value.

4.  $\mu_a^{(L)} \neq \mu_a^{(B)}$  and  $\mu_s'^{(L)} \neq \mu_s'^{(B)}$  (Different  $\mu_a$ , Different  $\mu_s'$ ) [Fig. 5(d)]

When the layer and the block differ in both the absorption and the reduced scattering coefficients,  $\mu_s'^{\text{(eff)}}$  measured with the frequency-domain multidistance method reproduces the block value if the layer thickness is less than  $\sim 0.5$  cm. The effective absorption coefficient  $\mu_a^{(\text{eff})}$  coincides with  $\mu_a^{(B)}$  for layer thicknesses less than 0.6 cm if the top layer is more scattering than the block and for thicknesses less than 0.25 cm if the layer is less scattering than the block. If the layer thickness exceeds 1.3 cm, the effective optical coefficients approach the values of the layer optical coefficients.

5. Summary of the Results when  $\mu_a^{(L)}$ ,  $\mu_s'^{(L)}$ , or Both Differ from the Block Coefficients

In Fig. 6 we show the deviations between the effective and the block coefficients, normalized by the deviations between the layer and the block coefficients. Specifically, the y axes of Figs. 6(a) and 6(b) are given by

$$\frac{\mu_a^{(\text{eff})} - \mu_a^{(B)}}{\mu_a^{(L)} - \mu_a^{(B)}}, \quad (8)$$

$$\frac{\mu_s'^{\text{(eff)}} - \mu_s'^{(B)}}{\mu_s'^{(L)} - \mu_s'^{(B)}}, \quad (9)$$

respectively. Figures 6(a) and 6(b) show only those cases for which  $\mu_a^{(L)} \neq \mu_a^{(B)}$  and  $\mu_s'^{(L)} \neq \mu_s'^{(B)}$ , respectively. Therefore the denominators in expressions (8) and (9) never get close to zero. As can be seen from expressions (8) and (9), these normalized deviations are 0 when the effective coefficients coincide with the block coefficients and they are 1 when the effective coefficients coincide with the coefficients of the layer. The x axis in Fig. 6 represents the dimensionless parameter  $t/\langle z \rangle_{\text{eff}}$ , where  $t$  is the layer

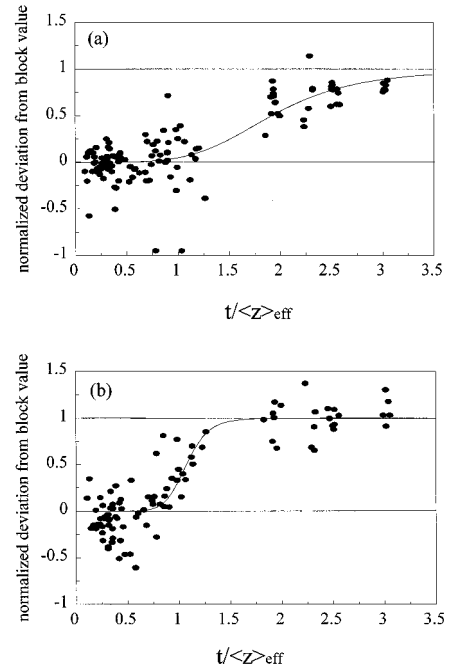


Fig. 6. Normalized deviations of (a) the effective absorption and (b) the reduced scattering coefficients from the corresponding block values. The symbols indicate the experimental results when the optical properties of the layer and the block were different. The curves give an indication of the average trend of the data points. These normalized deviations assume values of 0 and 1 when the measured effective coefficients coincide with those of the block and the layer, respectively. Horizontal axis, ratio between the thickness of the superficial layer ( $t$ ) and the average effective photon penetration depth ( $\langle z \rangle_{\text{eff}}$ ) calculated from Eq. (1). In the limit of very thin layers ( $t \rightarrow 0$ ), the normalized deviations tend to 0, indicating that we measure the optical properties of the underlying block. In the limit of a very thick superficial layer ( $t \rightarrow \infty$ ), the normalized deviations tend to 1, indicating that we measure the optical properties of the layer.

thickness and  $\langle z \rangle_{\text{eff}}$  is the average photon penetration depth computed with Eq. (1). To find  $\langle z \rangle_{\text{eff}}$  from Eq. (1) we used the effective optical coefficients [ $\mu_a^{(\text{eff})}$  and  $\mu_s'^{\text{(eff)}}$ ] and set the value of  $r$  to the average source–detector distance employed in our multidistance measurements. That is, we used  $r = 2.25$  cm for channel a and  $r = 3.75$  cm for channel b. The curves in Fig. 6 are an aid to the eye to indicate the average behavior of the data. These curves are empirically given by  $y = kx^\alpha / (1 + kx^\alpha)$  (where  $y$  and  $x$  indicate the vertical and horizontal axis variables, respectively), where  $k = 0.05$  and  $\alpha = 4.6$  in Fig. 6(a) (absorption) and  $k = 0.5$  and  $\alpha = 10$  in Fig. 6(b) (scattering). Figure 6 indicates the following: (1) The effective absorption coefficient reproduces the block absorption coefficient for values of  $t/\langle z \rangle_{\text{eff}}$  to  $\sim 1$ , whereas  $\mu_s'^{\text{(eff)}}$  reproduces  $\mu_s'^{(B)}$  only for  $t/\langle z \rangle_{\text{eff}}$  to  $\sim 0.8$ . This means that for a given value of  $\langle z \rangle_{\text{eff}}$  the block absorption coefficient can be accurately recovered in the presence of layers that are thicker than those required for accurate recovery of the reduced scattering coefficient of the block. (2) The transition between 0 and 1 for the normalized deviation occurs

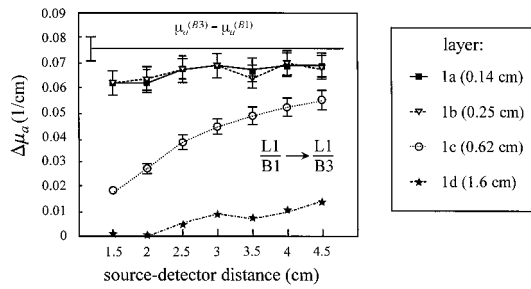


Fig. 7. Symbols represent the difference between the effective absorption coefficients measured with the precalibrated method on one layer from batch 1 on top of block 3 and on the same layer on top of block 1. Different symbols refer to different layer thicknesses. The horizontal line at  $0.076 \text{ cm}^{-1}$  indicates  $\mu_a^{(B3)} - \mu_a^{(B1)}$ .

on a much narrower range [in  $t/\langle z \rangle_{\text{eff}}$ ] for  $\mu_s'^{\text{(eff)}}$  than for  $\mu_a^{\text{(eff)}}$ . As a result, for a given value of  $\langle z \rangle_{\text{eff}}$ ,  $\mu_s'^{\text{(eff)}}$  recovers  $\mu_s'^{(L)}$  for thinner layers than required for  $\mu_a^{\text{(eff)}}$  to reproduce  $\mu_a^{(L)}$ . These results are consistent with the narrower spatial weight function for the reduced scattering coefficient with respect to that for the absorption coefficient.<sup>34</sup>

#### B. Relative Measurements of $\mu_a^{\text{(eff)}}$ (Frequency-Domain Precalibrated Method, Continuous-Wave Differential Path-Length Factor Method)

To perform relative measurements, i.e., measurements of differences in the effective absorption coefficient, we considered changes in the raw data (intensity and phase in the precalibrated method and intensity only in the DPF method) when the optical probe was moved from one layer–block configuration to another. We considered two cases: one in which we changed the underlying block and maintained the superficial layer unchanged (case A) and one in which we changed the layer and maintained the block unchanged (case B). By analyzing the data with the precalibrated and the DPF methods we were able to perform a relative absorption measurement for each source–detector distance ( $r$ ) in the range 1.5–4.5 cm. In Figs. 7 and 8 we show the relative effective absorption coefficient [ $\Delta\mu_a^{\text{(eff)}}$ ] as a function of  $r$  in case A (one layer from batch 1 on top of block 1 and one layer from batch 1 on top of block 3). For the two thinner layers ( $\leq 0.25 \text{ cm}$ ) the measured relative absorption coefficients do not show a dependence on  $r$ , and they are in reasonable agreement (within 13% for the precalibrated and 23% for the DPF methods) with  $\Delta\mu_a$  found on the blocks alone by the multidistance method [ $\mu_a^{(B3)} - \mu_a^{(B1)}$ ]. However, we note that the observed deviations are systematic and point out a limitation of the single-distance methods. For the thickest layer (1.6 cm) the measured  $\Delta\mu_a^{\text{(eff)}}$  is close to 0 because in this case light propagates mostly in the top layer (which is not changed in these case-A relative measurements). For the layer of intermediate thickness ( $\sim 0.62 \text{ cm}$ ) the measured relative absorption coefficient shows a strong dependence on  $r$  and approaches the value  $\mu_a^{(B3)} - \mu_a^{(B1)}$  at larger

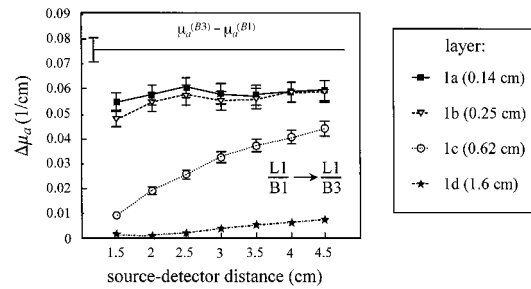


Fig. 8. Symbols represent the difference between the effective absorption coefficients measured with the DPF method on one layer from batch 1 on top of block 3 and on the same layer on top of block 1. Different symbols refer to different layer thicknesses. The horizontal line at  $0.076 \text{ cm}^{-1}$  indicates  $\mu_a^{(B3)} - \mu_a^{(B1)}$ .

source–detector distances. At the largest source–detector distance of 4.5 cm the recovered values of  $\Delta\mu_a^{\text{(eff)}}$  still differ by 30–40% from  $\mu_a^{(B3)} - \mu_a^{(B1)}$ . The results of the precalibrated method appear slightly better [in terms of the recovery of  $\mu_a^{(B3)} - \mu_a^{(B1)}$ ] than those of the DPF method because the assumptions in the latter method are stronger and less well satisfied [ $\mu_a^{\text{(eff)}}$  changes by 50% in the two measurements]. A qualitatively similar result was found in the case-B measurements, in which the two samples were composed of layer 1–block 1 and layer 3–block 1, respectively.

A comparison of the results for  $\Delta\mu_a^{\text{(eff)}}$  obtained with all three measurement protocols (frequency-domain multidistance, frequency-domain precalibrated, and cw DPF) is shown in Fig. 9 as a function of layer thickness. In this comparison we used the data at  $r = 4 \text{ cm}$  for the precalibrated and the DPF methods and the data in the range of distances 3.0–4.5 cm for the multidistance method. Figure 9(a) refers to case A (same layer, different block), and Fig. 9(b) refers to case B (different layer, same block). Figure 9 shows that the frequency-domain multidistance method is always the most effective, and it recovers the difference between the block absorption coefficients even in the presence of a superficial layer as much as 0.6 cm thick. This result confirms the predictions based on Fig. 3; namely, that the presence of a thin layer does not affect the slopes associated with dc and phase (which are used in the multidistance method), whereas it affects the intensity and the phase values at any value of  $r$  (which are used in the single-distance methods). Furthermore, the suggested dependence of the effective source terms on the optical properties<sup>32</sup> is another cause of error in single-distance methods.

## 6. Discussion and Conclusions

### A. Summary of Our Results

In discussing our results we must always keep in mind the particular conditions under which they were obtained. That is, the layer thickness was in the range 0.08–1.6 cm, the source–detector separation was in the range 1.5–4.5 cm, and the optical

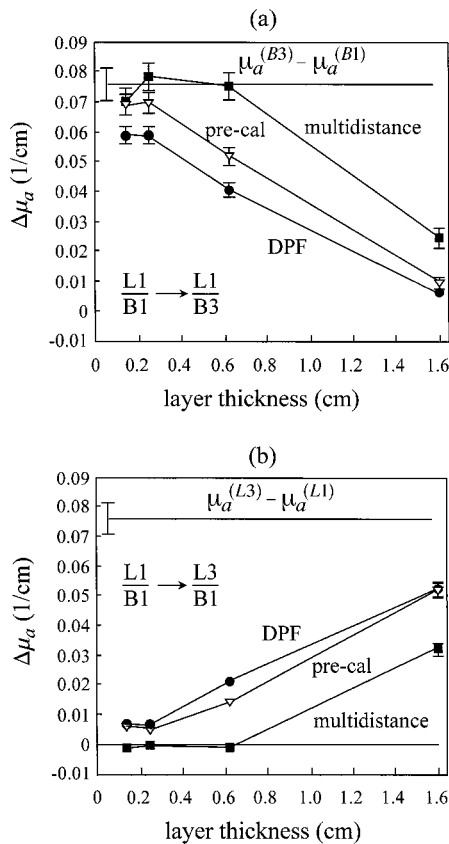


Fig. 9. Comparison of the relative measurements of  $\mu_a^{(\text{eff})}$  provided by the frequency-domain multidistance method ( $r$  in the range 3.0–4.5 cm; squares), the frequency-domain pre-calibrated method ( $r = 4$  cm; circles), and the cw DPF method ( $r = 4$  cm; triangles). (a) Only the block is changed [horizontal line,  $\Delta\mu_a^{(B)}$ ]. (b) Only the layer is changed [horizontal line,  $\Delta\mu_a^{(L)}$ ]. The multidistance method accurately recovers the difference between the block optical properties [ $\Delta\mu_a^{(B)}$  is 0 in (b)] even in the presence of a superficial layer as much as  $\sim 0.6$  cm thick.

properties were in the range  $0.070$ – $0.150 \text{ cm}^{-1}$  for  $\mu_a$  and  $9.2$ – $15.4 \text{ cm}^{-1}$  for  $\mu_s'$ . Under these conditions our major findings can be summarized as follows:

- For layer thicknesses less than  $\sim 0.4$  cm the frequency-domain multidistance method based on the diffusion theory for semi-infinite, homogeneous media yields effective optical coefficients that coincide with those of the underlying block. If the superficial layer is not significantly less scattering than the underlying block, the absorption coefficient of the block can be accurately measured even for thicker superficial layers, to  $\sim 0.6$  cm.

- If we consider larger source–detector distances, the frequency-domain multidistance method can quantify the block properties in the presence of thicker superficial layers. However, the reduction of the effect of the layer obtained by increasing  $r$  is not substantial within the range of distances considered by us.

- When the superficial layer is thicker than  $\sim 1.3$  cm the frequency-domain multidistance method

yields a reduced scattering coefficient that is representative of the layer. For the effective absorption coefficient to reproduce the layer absorption, the layer thickness should be larger ( $>1.5$  cm).

- Relative measurements of the effective absorption coefficient can be carried out with the cw DPF method, with the frequency-domain precalibrated method, and with the frequency-domain multidistance method. Also, in the case of relative measurements we found that to quantify the change in the absorption coefficient of the underlying block we require a layer thickness of less than  $\sim 0.4$  cm ( $\sim 0.6$  cm for the frequency-domain multidistance method). In the presence of a thin superficial layer the change in  $\mu_a^{(B)}$  was more accurately determined with the multidistance method than with the single-distance methods.

## B. Frequency-Domain Multidistance Method

The effectiveness of the frequency-domain multidistance method in quantifying the optical properties of the underlying block, even in the presence of a superficial layer, can be understood by the following argument: In this approach, as described by Eqs. (4) and (5),  $\mu_a^{(\text{eff})}$  and  $\mu_s^{(\text{eff})}$  are determined only by slopes  $S_{dc}$  and  $S_{\phi}$  of the functions  $f$  and  $h$  versus  $r$  [Eqs. (2) and (3)]. The presence of a thin layer that has different optical properties (let us say, a higher absorption) than the block will only cause a decrease in the intensity. Such a decrease will be similar at each source–detector separation, at least in the limiting case of a thin layer, and therefore will be indistinguishable from a decrease in the source power  $dc_0$ . A change in the source power influences only the intercept term  $K_{dc}$  and not the slope  $S_{dc}$  in Eq. (2). Our experimental results have addressed the question of how thin the superficial layer should be so it will not influence slopes  $S_{dc}$  and  $S_{\phi}$ .

One implication of our results is that quantitative spectroscopy of skeletal muscles with the multidistance method is accurate even in the presence of a skin–adipose layer as thick as  $\sim 0.4$  cm ( $\sim 0.6$  cm for the absorption coefficient). For greater thicknesses the absolute determination of the muscle's optical properties requires either larger source–detector separations or a refinement of the model. We can also draw another conclusion, based on a different perspective. A common criticism of quantitative tissue spectroscopy based on a semi-infinite, homogeneous medium model is the finite volume of tissues. For instance, it seems arguable to model the forearm of a thin person as a semi-infinite medium, given the small muscle volume and the proximity of the bones. However, if we look at the forearm muscle as a superficial layer, and the bone as the underlying medium, our research indicates that as long as the muscle is more than  $\sim 1.5$  cm thick the multidistance method (over distances in the range 1.5–4.5 cm) will accurately quantify its optical properties.

### C. Single-Distance Precalibrated and Differential Path-Length Factor Methods

Relative measurements of the absorption coefficient of the underlying medium can also be quantitative in the presence of thin superficial layers (thicknesses of  $\leq 0.3$  cm for the precalibrated and DPF methods and of  $\leq 0.6$  cm for the multidistance method). This result is relevant because the quantification of changes in absorption (quantitative relative measurements) can provide useful physiological information such as the local blood flow<sup>35</sup> and tissue oxygen consumption.<sup>36</sup> However, we found a systematic inaccuracy (10–20%) in the two single-distance methods, even in the presence of a thin superficial layer.

### D. Generalization of Our Results

Figure 6 gives indications about the extension of our results to a wider range of source–detector distances than the one considered in this paper. In fact, Fig. 6 describes how the effect of the layer on  $\mu_a^{(\text{eff})}$  and  $\mu_s^{(\text{eff})}$  scales with the thickness and the photon penetration depth. Furthermore, the dependence of the penetration depth ( $z$ ) on the square root of  $r$  indicates that to double ( $z$ ) one needs to increase  $r$  by a factor of 4. This result is consistent with our finding that, even though the range of distances 3.0–4.5 cm (channel b) proves to be less sensitive to the layer with respect to the range 1.5–3.0 cm (channel a), the improvement is not substantial.

We thank Alwin Kienle and Matthias Kohl for useful discussions on the diffusion-theory solution for two-layered media and on the DPF method, respectively. This research is supported by National Institutes of Health (NIH) grants CA57032, MH11432 and by Whitaker–NIH grant RR10966.

### References

1. B. Chance and R. R. Alfano, eds., *Optical Tomography and Spectroscopy of Tissue: Theory, Instrumentation, Model, and Human Studies II*, Proc. SPIE **2979** (1997).
2. D. A. Benaron, B. Chance, and M. Ferrari, eds., *Photon Propagation in Tissues III*, Proc. SPIE **3194** (1998).
3. H. Wallberg, A. Alveryd, K. Nasiell, P. Sundelin, U. Bergvall, and S. Troell, "Diaphanography in benign breast disorders: correlation with clinical examination, mammography, cytology and histology," *Acta Radiol. Diagn.* **26**, 129–136 (1985).
4. Y. Yamashita and M. Kaneko, "Visible and infrared diaphanoscropy for medical diagnosis," in *Medical Optical Tomography: Functional Imaging and Monitoring*, G. J. Muller, ed. (SPIE, Bellingham, Wash. 1993), pp. 283–316.
5. M. A. Franceschini, K. T. Moesta, S. Fantini, G. Gaida, E. Gratton, H. Jess, W. W. Mantulin, M. Seeber, P. M. Schlag, and M. Kaschke, "Frequency-domain techniques enhance optical mammography: initial clinical results," *Proc. Natl. Acad. Sci. USA* **94**, 6468–6473 (1997).
6. N. B. Hampson and C. A. Piantadosi, "Near infrared monitoring of human skeletal muscle oxygenation during forearm ischemia," *J. Appl. Physiol.* **64**, 2449–2457 (1988).
7. V. Quaresima, M. A. Franceschini, S. Fantini, E. Gratton, and M. Ferrari, "Difference in leg muscles oxygenation during treadmill exercise by a new near infrared frequency-domain oximeter," in *Photon Propagation in Tissues III*, D. A. Benaron, B. Chance, and M. Ferrari, eds., Proc. SPIE **3194**, 116–120 (1998).
8. S. Homma, T. Fukunaga, and A. Kagaya, "Influence of adipose tissue thickness on near infrared spectroscopic signals in the measurement of human muscle," *J. Biomed. Opt.* **1**, 418–424 (1996).
9. S. P. Gopinath, C. S. Robertson, R. G. Grossman, and B. Chance, "Near-infrared spectroscopic localization of intracranial hematomas," *J. Neurosurg.* **79**, 43–47 (1993).
10. G. Gratton, M. Fabiani, D. Friedman, M. A. Franceschini, S. Fantini, P. M. Corballis, and E. Gratton, "Rapid changes of optical parameters in the human brain during a tapping task," *J. Cogn. Neurosci.* **7**, 446–456 (1995).
11. M. S. Patterson, B. Chance, and B. C. Wilson, "Time resolved reflectance and transmittance for the non-invasive measurement of optical properties," *Appl. Opt.* **28**, 2331–2336 (1989).
12. S. Fantini, M. A. Franceschini, J. S. Maier, S. A. Walker, B. Barbieri, and E. Gratton, "Frequency-domain multichannel optical detector for non-invasive tissue spectroscopy and oximetry," *Opt. Eng.* **34**, 32–42 (1995).
13. M. Miwa, Y. Ueda, and B. Chance, "Development of time resolved spectroscopy system for quantitative non-invasive tissue measurement," in *Optical Tomography, Photon Migration, and Spectroscopy of Tissue and Model Media: Theory, Human Studies, and Instrumentation*, B. Chance and R. R. Alfano, eds., Proc. SPIE **2389**, 142–149 (1995).
14. J. B. Fishkin, O. Coquoz, E. R. Anderson, M. Brenner, and B. J. Tromberg, "Frequency-domain photon migration measurements of normal and malignant tissue optical properties in a human subject," *Appl. Opt.* **36**, 10–20 (1997).
15. J. S. Maier, S. A. Walker, S. Fantini, M. A. Franceschini, and E. Gratton, "Possible correlation between blood glucose concentration and the reduced scattering coefficient of tissues in the near infrared," *Opt. Lett.* **19**, 2062–2064 (1994).
16. M. Kohl, M. Cope, M. Essenpreis, and D. Böcker, "Influence of glucose concentration on light scattering in tissue-simulating phantoms," *Opt. Lett.* **19**, 2170–2172 (1994).
17. J. T. Bruulsema, J. E. Hayward, T. J. Farrel, M. S. Patterson, L. Heinemann, M. Berger, T. Koschinsky, J. Sandahl-Christiansen, H. Orskov, M. Essenpreis, G. Schmelzeisen-Redeker, and D. Böcker, "Correlation between blood glucose concentration in diabetics and noninvasively measured tissue optical scattering coefficient," *Opt. Lett.* **22**, 190–192 (1997).
18. R. Nossal, J. Kiefer, G. H. Weiss, R. Bonner, H. Taitelbaum, and S. Havlin, "Photon migration in layered media," *Appl. Opt.* **27**, 3382–3391 (1988).
19. H. Taitelbaum, S. Havlin, and G. H. Weiss, "Tissue characterization and imaging using photon density waves," *Appl. Opt.* **28**, 2245–2249 (1989).
20. M. Keijzer, W. M. Star, and P. R. M. Storchi, "Optical diffusion in layered media," *Appl. Opt.* **27**, 1820–1824 (1988).
21. J. M. Schmitt, G. X. Zhou, E. C. Walker, and R. T. Wall, "Multilayer model of photon diffusion in skin," *J. Opt. Soc. Am. A* **7**, 2141–2153 (1990).
22. I. Dayan, S. Havlin, and G. H. Weiss, "Photon migration in a two-layer turbid medium: a diffusion analysis," *J. Mod. Opt.* **39**, 1567–1582 (1992).
23. A. Kienle, M. S. Patterson, N. Dögnitz, R. Bays, G. Wagnières, and H. van den Bergh, "Noninvasive determination of the optical properties of two-layered turbid media," *Appl. Opt.* **37**, 779–791 (1998).
24. T. J. Farrel, M. S. Patterson, and M. Essenpreis, "Influence of layered tissue architecture on estimates of tissue optical properties obtained from spatially resolved diffuse reflectometry," *Appl. Opt.* **37**, 1958–1972 (1998).
25. A. H. Hielscher, H. Liu, L. Wang, F. K. Tittel, B. Chance, and S. L. Jacques, "Determination of blood oxygenation in the brain by time resolved reflectance spectroscopy. I. Infl-

- ence of the skin, skull, and meninges," in *Biochemical Diagnostic Instrumentation*, R. F. Bonner, G. E. Cohn, T. M. Laue, and A. V. Priezzhev, eds., Proc. SPIE **2136**, 15–25 (1994).
26. A. Cerussi, J. Maier, S. Fantini, M. A. Franceschini, and E. Gratton, "The frequency-domain multi-distance method in the presence of curved boundaries," OSA Trends in Optics and Photonics on *Biomedical Optical Spectroscopy and Diagnostics*, E. Sevick-Muraca and D. Benaron, eds., Vol. 3 of OSA Trends in Optics and Photonics Series (Optical Society of America, Washington, D.C., 1996), pp. 92–97.
  27. M. S. Patterson, S. Andersson-Engels, B. C. Wilson, and E. K. Osei, "Absorption spectroscopy in tissue-simulating materials: a theoretical and experimental study of photon paths," *Appl. Opt.* **34**, 22–30 (1995).
  28. M. A. Franceschini, D. Wallace, B. Barbieri, S. Fantini, W. W. Mantulin, S. Pratesi, G. P. Donzelli, and E. Gratton, "Optical study of the skeletal muscle during exercise with a second generation frequency-domain tissue oximeter," in *Optical Tomography and Spectroscopy of Tissue: Theory, Instrumentation, Model, and Human Studies II*, B. Chance and R. R. Alfano, eds., Proc. SPIE **2979**, 807–814 (1997).
  29. S. Fantini, M. A. Franceschini, and E. Gratton, "Semi-infinite-geometry boundary problem for light migration in highly scattering media: a frequency-domain study in the diffusion approximation," *J. Opt. Soc. Am. B* **11**, 2128–2138 (1994).
  30. S. Fantini, M. A. Franceschini, J. B. Fishkin, B. Barbieri, and E. Gratton, "Quantitative determination of the absorption spectra of chromophores in strongly scattering media: a light-emitting-diode based technique," *Appl. Opt.* **33**, 5204–5213 (1994).
  31. M. A. Franceschini, S. Fantini, S. A. Walker, J. S. Maier, W. W. Mantulin, and E. Gratton, "Multi-channel optical instrument for near-infrared imaging of tissue," in *Optical Tomography, Photon Migration, and Spectroscopy of Tissue and Model Media: Theory, Human Studies, and Instrumentation*, B. Chance and R. R. Alfano, eds. Proc. SPIE **2389**, 264–273 (1995).
  32. S. Fantini, M. A. Franceschini, and E. Gratton, "Effective source term in the diffusion equation for photon transport in turbid media," *Appl. Opt.* **36**, 156–163 (1997).
  33. M. Cope, P. van der Zee, M. Essenpreis, S. R. Arridge, and D. T. Delpy, "Data analysis methods for near infrared spectroscopy of tissues: problems in determining the relative cytochrome  $aa_3$  concentration," in *Time-Resolved Spectroscopy and Imaging of Tissues*, B. Chance, ed., Proc. SPIE **1431**, 251–263 (1991).
  34. S. Fantini, M. A. Franceschini, S. A. Walker, J. S. Maier, and E. Gratton, "Photon path distributions in turbid media: applications for imaging," in *Optical Tomography, Photon Migration, and Spectroscopy of Tissue and Model Media: Theory, Human Studies, and Instrumentation*, B. Chance and R. R. Alfano, eds., Proc. SPIE **2389**, 340–349 (1995).
  35. A. D. Edwards, C. Richardson, P. Van der Zee, C. Elwell, J. S. Wyatt, M. Cope, D. T. Delpy, and E. O. R. Reynolds, "Measurement of hemoglobin flow and blood flow by near-infrared spectroscopy," *J. Appl. Physiol.* **75**, 1884–1889 (1993).
  36. R. A. de Blasi, M. Cope, C. Elwell, F. Safoue, and M. Ferrari, "Non invasive measurement of human forearm oxygen consumption by near infrared spectroscopy," *Eur. J. Appl. Physiol.* **67**, 20–25 (1993).